# Proposal for Observing Yang-Lee Criticality in Rydberg Atomic Arrays

Ruizhe Shen,[1,*] Tianqi Chen,[2,†] Mohammad Mujahid Aliyu,[3,‡] Fang Qin (覃昉),[1] Yin Zhong,[4,5] Huanqian Loh,[1,3,§] and Ching Hua Lee[1,6,‖]

[1]*Department of Physics, National University of Singapore, Singapore 117551, Singapore*
[2]*School of Physical and Mathematical Sciences, Nanyang Technological University, Singapore 639798, Singapore*
[3]*Centre for Quantum Technologies, National University of Singapore, 117543 Singapore, Singapore*
[4]*School of Physical Science and Technology and Key Laboratory for Magnetism and Magnetic Materials of the MoE, Lanzhou University, Lanzhou 730000, China*
[5]*Lanzhou Center for Theoretical Physics, Key Laboratory of Theoretical Physics of Gansu Province, Lanzhou 730000, China*
[6]*Joint School of National University of Singapore and Tianjin University, International Campus of Tianjin University, Binhai New City, Fuzhou 350207, China*

(Received 24 February 2023; revised 27 June 2023; accepted 25 July 2023; published 25 August 2023)

Yang-Lee edge singularities (YLES) are the edges of the partition function zeros of an interacting spin model in the space of complex control parameters. They play an important role in understanding non-Hermitian phase transitions in many-body physics, as well as characterizing the corresponding nonunitary criticality. Even though such partition function zeroes have been measured in dynamical experiments where time acts as the imaginary control field, experimentally demonstrating such YLES criticality with a physical imaginary field has remained elusive due to the difficulty of physically realizing non-Hermitian many-body models. We provide a protocol for observing the YLES by detecting kinked dynamical magnetization responses due to broken $\mathcal{PT}$ symmetry, thus enabling the physical probing of nonunitary phase transitions in nonequilibrium settings. In particular, scaling analyses based on our nonunitary time evolution circuit with matrix product states accurately recover the exponents uniquely associated with the corresponding nonunitary CFT. We provide an explicit proposal for observing YLES criticality in Floquet quenched Rydberg atomic arrays with laser-induced loss, which paves the way towards a universal platform for simulating non-Hermitian many-body dynamical phenomena.

DOI: 10.1103/PhysRevLett.131.080403

*Introduction.*—In 1952, Yang and Lee established a relationship between phase transitions and special points where the partition function vanishes, also known as Yang-Lee zeros [1,2]. For a spin model in the thermodynamic limit, nonunitary critical points known as Yang-Lee edge singularities (YLES) [3–6] lie at the ends of a dense line of partition function zeros in the space of complex control parameters such as the magnetic field or inverse temperature [1,2]. To observe YLES, one can examine a non-Hermitian quantum ferromagnetic many-body Hamiltonian involving complex magnetic fields [5–8]. The YLES of such non-Hermitian ferromagnetic models lead to anomalous critical scaling behaviors associated with their governing nonunitary conformal field theories (CFTs) [6,8,9].

For a long time, Yang-Lee edge singularities, requiring challenging experimental realization of imaginary fields, have been deemed as purely theoretical constructs. Recently, it was realized that the partition function of a classical spin model can also be mathematically simulated by real-time evolution, and Yang-Lee zeros were finally observed through probing spin coherence in a series of landmark experiments involving externally coupled local spins [10–12]. However, what these experiments achieved was the measurement of partition function zeros through a dynamical process, not the physical observation of the YLES and their associated nonunitary phase transition. It is still difficult to realize such esoteric phenomena in a finite-size quantum ferromagnetic model with physical complex fields. While various single-body non-Hermitian phenomena have already been demonstrated [13–15], experimental demonstrations in *interacting* many-body non-Hermitian models have just begun, primarily with cold atoms [16–20].

Indeed, ultracold atomic systems have lately proven to be ideal platforms for simulating many-body physics due to their excellent tunability and high controllability [21–26], with demonstrated successes in topological physics [27,28], strongly correlated matter [29–31], and thermalization phenomena [32,33]. Rydberg atomic arrays are particularly promising, with Rydberg interactions successfully deployed to simulate many-body Hamiltonians [34–42]. Rydberg-dressing techniques offer new possibilities for engineering complex many-body phases due to their great tunability in shaping interactions [43–51]. To introduce non-Hermiticity in an ultracold atomic lattice, an increasingly established approach [19,20,52–56] is laser-induced loss by exciting atoms to "external" states [18,19,57]. Encouraged by these

 

recent rapid advances in ultracold atoms, we combine Rydberg-dressing techniques with laser-induced loss to realize a ferromagnetic chain with an imaginary effective field, such as to observe the YLES in a genuinely physical complex parameter space.

In this work, we first introduce a transverse-field Ising model with imaginary fields and discuss its critical signatures associated with spontaneous $\mathcal{PT}$ breaking [58–61]. We next devise a Floquet quench for observing the YLES phase boundary by measuring nonequilibrium kinked responses, before describing our proposed experiment involving a dissipative Rydberg-dressed optical tweezer array [6,45,46,50,62], where the imaginary field is implemented through laser-induced atom loss [18,19,57].

*Model for Yang-Lee edge singularities.*—For a concrete platform for observing Yang-Lee criticality, we consider the prototypical non-Hermitian ferromagnetic transverse-field Ising chain [63,64], which we will later show the realization in Rydberg atoms:

$$\hat{H}_{\mathrm{TFI}} = -\sum_j (h_x \hat{\sigma}_j^x + J\hat{\sigma}_j^z \hat{\sigma}_{j+1}^z) + \sum_j i\gamma \hat{\sigma}_j^z, \qquad (1)$$

where $J$ sets the strength of the interaction, $\gamma$ is the imaginary field strength. and $\hat{\sigma}_j^\alpha (\alpha = x, z)$ are Pauli matrices. The YLES for this model form a curve in the plane of real and imaginary magnetic fields $(h_x, \gamma)$ in Fig. 1(a) [6], which we denote as $\gamma_{\mathrm{YL}}$ at each value of $h_x$. When approaching $\gamma_{\mathrm{YL}}$, the ground states of our model experience spontaneous $\mathcal{PT}$ symmetry breaking [6], with real ground-state eigenenergies $E_g$ splitting into complex eigenenergies with equal and opposite $\mathrm{Im}E_g$, which demarcate the paramagnetic and ferromagnetic ground states in our model, as shown in Fig. 1(a) for $\hat{H}_{\mathrm{TFI}}$: the paramagnetic (ferromagnetic) phases are characterized by vanishing (nonvanishing) $\mathrm{Im}E_g$.

Despite YLES initially being defined for classical systems in the thermodynamic limit, they equivalently exist in finite-size quantum systems due to a quantum-classical mapping [3,4,6,9,65–69], as shown in Figs. 1(a) and 1(b), which were computed through exact diagonalization (ED) with $L = 8$ sites. In Figs. 1(c) and 1(d), the associated ground state magnetization $M_z = |\langle \sum_j \hat{\sigma}_j^z / L \rangle|$ and $M_x = |\langle \sum_j \hat{\sigma}_j^x / L \rangle|$ also exhibit kinks at these YLES locations. Indeed, comparing the derivatives $\{d|[\mathrm{Im}E_g(\gamma)]|/d\gamma\}$ against that of the $x$ magnetization $|dM_x(\gamma)/d\gamma|$ [Fig. 1(d)], we observe divergences at the same YLES $\gamma = \gamma_{\mathrm{YL}} = 0.1837$ (for $J = 1$, $h_x = 1.5$).

*Dynamical response from Yang-Lee edge singularities.*—Since Eq. (1) is non-Hermitian, any physical realization will undergo nonequilibrium evolution, making it difficult to directly probe ground state properties such as Yang-Lee criticality via a static ensemble measurement. A nonequilibrium detection of ground state transitions

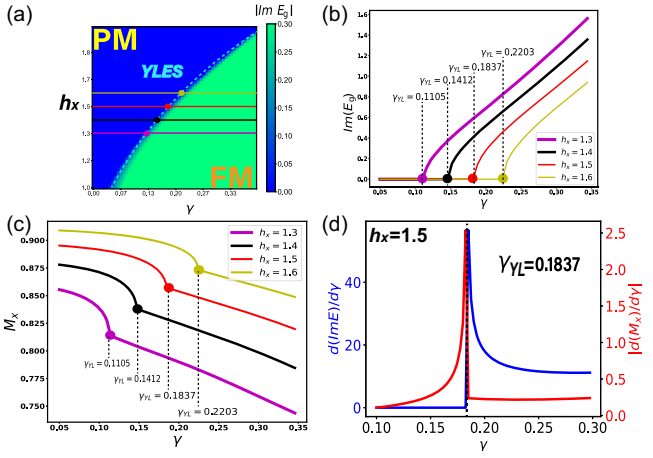


FIG. 1. Theoretical characterization of the Yang-Lee edge singularities of $\hat{H}_{\mathrm{TFI}}$ [Eq. (1)] and their associated ground state discontinuities: (a) Phase diagram of $\hat{H}_{\mathrm{TFI}}$ in the space of real and complex fields $h_x$ and $\gamma$. The YLES (dashed curve) is the phase boundary demarcating the paramagnetic (PM) $\mathrm{Im}E_g = 0$ phase and the ferromagnetic (FM) $|\mathrm{Im}E_g| > 0$ phase, where $E_g$ is the ground state eigenenergy with the minimal real part. (b) Plots of $\mathrm{Im}E_g$ vs $\gamma$ at the four values of $h_x$ indicated in (a), revealing that $E_g$ is nonanalytic at YLES $\gamma_{YL}$. (c) Identification of Yang-Lee phase transitions by the ground state magnetization order parameter $M_x = |\langle \sum_j \hat{\sigma}_j^x / L \rangle|$. Magnetization kinks (dashed lines) occur at the same $\gamma_{\mathrm{YL}}$ as in (b). (d) The critical point (at $\gamma_{\mathrm{YL}} = 0.1837$ for $h_x = 1.5$) can be equivalently extracted from divergences in either the derivative of the imaginary ground state energy $\{d|\mathrm{Im}[E_g(\gamma)]|/d\gamma\}$ (blue), or that of the ground state $x$ magnetization $(dM_x/d\gamma)$ (red). All results are obtained from exact diagonalization (ED) with open boundary conditions, with interaction strength $J = 1$ and system size $L = 8$.

requires different behaviors across phases, in particular with one dominating the dynamics [6,70–72].

To probe the YLES dynamically, we turn to the spectral flow across critical points. The underappreciated but crucial observation is that due to $\mathcal{PT}$-symmetry breaking, imaginary eigenenergies appear and that leads to markedly different nonunitary dynamics across the transition [6]. From Fig. 2(a), the ground state energy $E_g$ (with smallest $\mathrm{Re}E_g$) is seen to rapidly acquire larger $\pm\mathrm{Im}E_g$ immediately after $\gamma$ is tuned to be greater than $\gamma_{\mathrm{YL}}$ (inset). By contrast, other nonground state eigenenergies in Fig. 2(a) are largely stationary. This drastic real-to-complex ground state eigenenergy transition does not just imply that ground state observables, i.e., $M_x$ exhibit a kink at the YLES—more importantly, the rapidly increasing $\mathrm{Im}E_g$ at $\gamma > \gamma_{\mathrm{YL}}$ suggests that upon time evolution by $\hat{H}_{\mathrm{TFI}}$, *any* initial state with significant ground state overlap will converge towards the ground state and dominate.

As such, our proposal to experimentally detect nonunitary critical YLES involves measuring the dynamical $x$-magnetization order parameter $M_x(T) = \langle \psi(t)| \sum_j \hat{\sigma}_j^x / L |\psi(t)\rangle$, which we henceforth expect to exhibit similar kinks as the

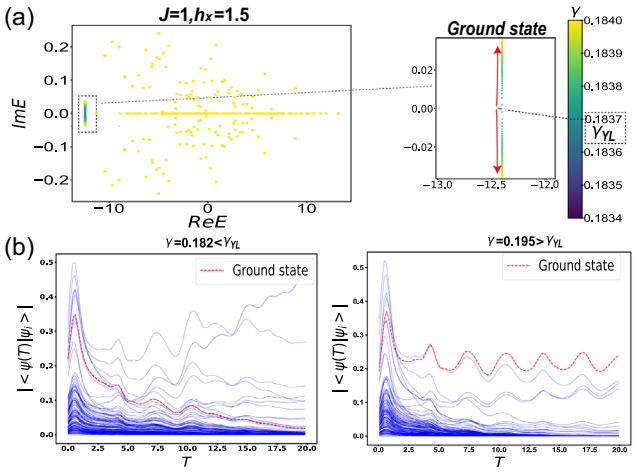


FIG. 2. (a) Flow of the complex spectrum of $\hat{H}_{\mathrm{TFI}}$ [Eq. (1)] as $\gamma$ is tuned across $\gamma_{\mathrm{YL}} \approx 0.1837$. The ground state eigenenergies (boxed) undergo spontaneous $\mathcal{PT}$ symmetry breaking and rapidly acquire imaginary parts (green to yellow, red arrow) as $\gamma$ increases slightly above $\gamma_{\mathrm{YL}}$, much more so than other eigenenergies. (b) and (c): Evolution of the overlap $|\langle\psi(T)|\psi_i\rangle|$ between the dynamically evolved state $|\psi(T)\rangle = e^{-iT\hat{H}_{\mathrm{TFI}}}|\psi(0)\rangle/\|e^{-iT\hat{H}_{\mathrm{TFI}}}|\psi(0)\rangle\|$ and all eigenstates $|\psi_i\rangle$ (blue) of $\hat{H}_{\mathrm{TFI}}$, with initial state being $|\psi(0)\rangle = |\downarrow\downarrow\ldots\ldots\rangle$. For $\gamma$ below the YLES $\gamma_{\mathrm{YL}}$ (b), the ground state overlap (red dashed) decreases rapidly due to mixing. But for $\gamma > \gamma_{\mathrm{YL}}$, the ground state component becomes dominant beyond time $TJ \sim \mathcal{O}(10)$ due to the large $\mathrm{Im}E_g$ of the ground state, leading to kinked magnetization responses detectable in our proposed Rydberg atom system of Fig. 4 below. All results are obtained from ED with $J = 1$, $h_x = 1.5$, and $L = 8$.

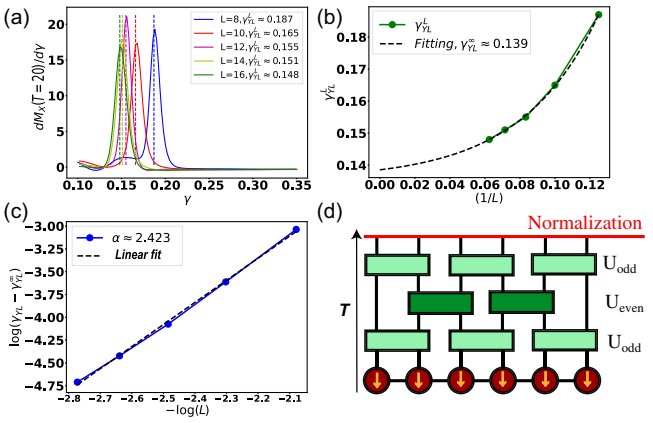


FIG. 3. Anomalous critical scaling of dynamically determined Yang-Lee edge singularities of $\hat{H}_{\mathrm{TFI}}$, with $J = 1$ and $h_x = 1.5$. (a) Size-dependent YLES $\gamma^L_{\mathrm{YL}}$ as kinks in the derivative $[dM_x(T)/d\gamma]$. The dynamical magnetization $M_x(T) = |\langle\psi(T)|\sum_j \hat{\sigma}^x_j|\psi(T)\rangle|/L$ is measured at time $T = 20/J$ for different system sizes $L = 8$ to 16 using our tMPS algorithm from (d). (b) Extrapolation of $\gamma^L_{\mathrm{YL}}$ with $1/L$ gives the thermodynamic limit YLES value $\gamma^\infty_{\mathrm{YL}} \approx 0.139$ through polynomial fitting. (c) Plotting our data for $\log(\gamma^L_{\mathrm{YL}} - \gamma^\infty_{\mathrm{YL}})$ against $-\log L$ yields the critical exponent $\alpha \approx 2.423$ as the gradient [Eq. (2)], which agrees closely with the CFT result $\alpha = 12/5$ [75,76]. (d) The nonunitary circuit for implementing the time evolution of our model [6], where each step is decomposed into odd-bond $U_{\mathrm{odd}}$ (light green) and even-bond $U_{\mathrm{even}}$ (dark green) parts, with normalization (red solid line) performed at the end.

ground state $M_x$ [Fig. 1(c)]. The edge of such nonunitary phase transitions can be identified by plotting the kink locations of $M_x(T)$ in parameter space. With our Rydberg array implementation in mind, we propose the following protocol: (1) Prepare an ordered initial state $|\psi(0)\rangle = |\downarrow\downarrow\ldots\ldots\rangle$. [73] (2) Apply quench dynamics on this ordered initial state, resulting in normalized result: $|\psi(t)\rangle = e^{-it\hat{H}_{\mathrm{TFI}}}|\psi(0)\rangle/\|e^{-it\hat{H}_{\mathrm{TFI}}}|\psi(0)\rangle\|$ with $\||\psi\rangle\| = \sqrt{|\langle\psi|\psi\rangle|}$. (3) Measure the $x$ magnetization order parameter $M_x(T) = |\langle\psi(T)|\sum_j \hat{\sigma}^x_j|\psi(T)\rangle|/L$ after a sufficiently long stipulated time $T$ for different $\gamma$, keeping $J$ and $h_x$ fixed. As shown in Figs. 2(b) and 2(c), the initial ferromagnetic state $|\psi(0)\rangle$ already overlaps with the ground state of $\hat{H}_{\mathrm{TFI}}$ more than most other eigenstates. Because of the PT-symmetry breaking, after evolving for $TJ \sim \mathcal{O}(10^1)$, it is dominated by the ground state for $\gamma > \gamma_{\mathrm{YL}}$, but not when $\gamma < \gamma_{\mathrm{YL}}$. As such, we expect to observe a kink in $M_x(T)$ across the critical YLES $\gamma = \gamma_{\mathrm{YL}}$, even though there is considerable ground state overlap at one side of the transition. Note that even though the ground state $M_x(T)$ is extracted through a dynamical quench, what we are measuring is not mathematically a dynamical phase transition [10–12,74]. Instead, our proposal for measuring nonunitary criticality can be demonstrated by our designed experimental optical arrays discussed below.

*Nonunitary criticality of Yang-Lee edge singularities.*— We then demonstrate how to determine the YLES critical exponents using finite-size scaling with our protocol. After fixing the quenching duration $T$, the critical values $\gamma = \gamma^L_{\mathrm{YL}}$ at different $L$ can be extracted from the peak divergences of the plots of the derivative of $M_x(T)$ with respect to $\gamma$. This is illustrated in Fig. 3(a) with data from our tMPS simulation (described shortly after), computed with $T = 20/J$ with $J = 1$ [6]. Here, for different system sizes $L = 8, 10, \ldots, 16$, the critical values of $\gamma = \gamma^L_{\mathrm{YL}}$ are marked by dashed vertical lines, where the derivatives peak. In an experiment, $\gamma^L_{\mathrm{YL}}$ can be extracted by adjusting $\gamma$ and measuring $M_x(T)$ in separate spin chains of various lengths $L$.

The characteristic critical exponents for the YLES can be extracted via the following universal critical scaling law of its nonunitary $c = -22/5$ conformal field theory (CFT) [9,77]:

$$\gamma^L_{\mathrm{YL}} - \gamma^\infty_{\mathrm{YL}} \propto L^{-\alpha} = L^{-(\beta_1\delta_1/\nu_1)}, \tag{2}$$

where $\gamma^L_{\mathrm{YL}}$ is the location of the YLES obtained from our protocol at finite size $L$. $\gamma^\infty_{\mathrm{YL}}$ represents the YLES as $L \to \infty$, which can be obtained from our finite-sized data by extrapolating $\gamma^L_{\mathrm{YL}}$ with respect to $1/L$, as performed by polynomial fitting in Fig. 3(b). Upon obtaining $\gamma^\infty_{\mathrm{YL}}$, one

can further plot $\log(\gamma_{\rm YL}^{L}-\gamma_{\rm YL}^{\infty})$ against $\log(1/L)$, such that the critical exponent $\alpha$ in Eq. (2) can be extracted from the gradient of the fitted line in Fig. 3(c). Such nonunitary CFT behavior, which has been elusive in experiments, can be readily measured in our proposed cold atom setup. Our tMPS result $\alpha_{\rm MPS}\approx 2.423$ is in excellent agreement with the theoretical value from the nonunitary CFT with central charge $c=-22/5$ for the YLES: $\alpha_{\rm CFT}=\beta_1\delta_1/\nu_1=2.40$ with $\beta_1=1$, $\delta_1=-6$, $\nu_1=-5/2$ [75,76].

Before discussing the detailed experimental process, we briefly describe our designed nonunitary numerical algorithm for the results in Fig. 3, which is built upon the state-of-art matrix product states (tMPS) tool for handling generic one-dimensional quantum many-body systems with nearest-neighbor couplings [78–81]. As sketched in Fig. 3(d) [82], we build a nonunitary circuit for $e^{-i\delta t\hat{H}_{\rm TFI}}$ [6,83–85], which is implemented through a second-order Suzuki-Trotter decomposition built by nonunitary even and odd bonds [6]. A key feature is that normalization at the end of each time step suppresses numerical divergences, facilitating the precise computation of long-time dynamics ($T=30$) [6]. Therefore, our method offers direct, efficient implementations, outperforming ancilla-based approaches with significant information wastage and poor scalability [83,86].

*Experimental proposal with Rydberg atoms.*—We then show how to implement the dynamics $e^{-iT\hat{H}_{\rm TFI}}$ to observe the YLES through our driving protocol in Rydberg atomic arrays. Given that in a Rydberg system [19,50], the implementation of transverse fields $\hat{H}_X(F)=-\sum_j F\hat{\sigma}_j^x$, atomic loss $\hat{H}_Z(g)=-i\sum_j g\hat{\sigma}_j^z$ and, ferromagnetic interactions $\hat{H}_{ZZ}=-\sum_j J_0\hat{\sigma}_i^z\hat{\sigma}_{i+1}^z$ are all feasible, we can Trotterize $e^{-iT\hat{H}_{\rm TFI}}$ into $N$ periods by a two-step Floquet driving protocol (Fig. 4)

$$e^{-iT\hat{H}_{\rm TFI}}\approx\left[e^{+i\tau_x\hat{H}_X(F)+i\tau_\gamma\hat{H}_Z(g)}e^{+i\tau_J\hat{H}_{ZZ}}\right]^N=[U_2^{\rm Floq}U_1^{\rm Floq}]^N,\tag{3}$$

where $U_1^{\rm Floq}=e^{i\tau_J\hat{H}_{ZZ}}$ followed by $U_2^{\rm Floq}=e^{i\tau_x\hat{H}_X(F)+i\tau_\gamma\hat{H}_Z(g)}$, and the physical magnitudes $F$, $g$, and $J_0$ are related to their corresponding quenching durations $\tau_J$, $\tau_x$, and $\tau_\gamma$ via $(\tau_xF,\tau_\gamma g,\tau_JJ_0)=(T/N)(h_x,\gamma,J)$. The Floquet cycles $N=(TJ/J_0\tau_J)$ needs to be determined under the condition of coherent dynamics [87].

We next detail the experimental Floquet quenches $U_1^{\rm Floq}$ and $U_2^{\rm Floq}$ in our Rydberg setup, built by the pseudospin-1/2 of two hyperfine Caesium ground states: $|\downarrow\rangle=|6S_{1/2},F=3,m_F=+3\rangle$ and $|\uparrow\rangle=|6S_{1/2},F=4,m_F=+4\rangle$ (Fig. 4) [6]. To engineer interactions in the first step $U_1^{\rm Floq}$, we couple the state $|\uparrow\rangle$ with the Rydberg state $|60P_{3/2},m_J=+3/2\rangle$ under large detuning $\Delta$ vs Rabi frequency $\Omega$ (blue arrow in Fig. 4) [6]. Consequently, the Rydberg-dressing process leads to an energy shift of

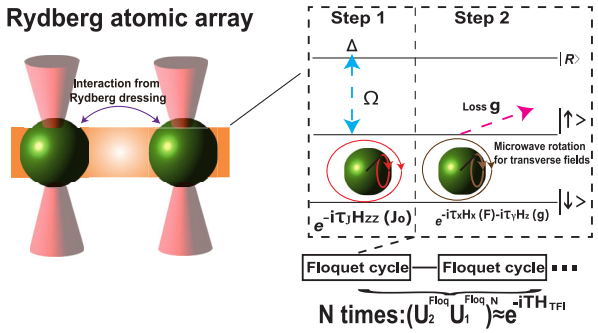


FIG. 4. Proposed Rydberg atomic array for realizing the Floquet drives $U_1^{\rm Floq}$ and $U_2^{\rm Floq}$ in Eq. (3). Optical tweezers (red, left) trap Cesium atoms (green), with their two hyperfine ground states defining pseudospin-1/2 states $|\downarrow\rangle=|6S_{1/2},F=3,m_F=+3\rangle$ and $|\uparrow\rangle=|6S_{1/2},F=4,m_F=+4\rangle$ (right). In $U_1^{\rm Floq}$ (Step 1), $\Omega$ driving (blue dashed arrow) couples $|\uparrow\rangle$ and the Rydberg state $|60P_{3/2},m_J=+3/2\rangle$, resulting in a Rydberg-dressed nearest-neighbor $|\uparrow\uparrow\rangle$ interaction $\hat{H}_{\rm int}$ (purple arrow) that can be converted to a ferromagnetic interaction via spin echo (red loop). In $U_2^{\rm Floq}$ (Step 2), a microwave field (brown loop) generates the transverse field $F\hat{\sigma}^x$, while a laser couples $|\uparrow\rangle\rightarrow|6P_{3/2},F=5,m_F=+5\rangle$, resulting in the imaginary field $ig\hat{\sigma}^z$ [6]. The quenching durations $\tau_J$, $\tau_x$ and $\tau_\gamma$ are chosen such that $(\tau_xF,\tau_\gamma g,\tau_JJ_0)=(T/N)(h_x,\gamma,J)$.

$J_0\approx(\Omega^4/8\Delta^3)$ in the nearest-neighbor subspace $|\uparrow\uparrow\rangle_{i,i+1}$, resulting in effective interactions [6,44,102]

$$\hat{H}_{\rm int}(J_0)=-\sum_i J_0\hat{P}_i\hat{P}_{i+1},\tag{4}$$

where $\hat{P}_i=[(\hat{\sigma}_i^z+\hat{I}_i)/2]$ with $\hat{\sigma}_i^z=|\uparrow\rangle_i\langle\uparrow|_i-|\downarrow\rangle_i\langle\downarrow|_i$ and $\hat{I}_i=|\uparrow\rangle_i\langle\uparrow|_i+|\downarrow\rangle_i\langle\downarrow|_i$. While this is still not the ferromagnetic interaction required in $\hat{H}_{\rm TFI}$ of Eq. (3), inspired by the operator identity $e^{-i(\pi/2)\hat{\sigma}^x}e^{i\tau_JJ_0\hat{\sigma}^z}e^{-i(\pi/2)\hat{\sigma}^x}e^{i\tau_JJ_0\hat{\sigma}^z}=-\hat{I}$, one can convert it into a clean ferromagnetic interaction $\hat{H}_{ZZ}(J_0)=-\sum_j J_0\hat{\sigma}_i^z\hat{\sigma}_{i+1}^z$, by applying two transverse $\hat{\sigma}^x$ field kicks:

$$(e^{-i(\pi/2)\sum_j\hat{\sigma}_j^x}e^{i\tau_J\hat{H}_{\rm int}(2J_0)})^2\approx U_1^{\rm Floq},\tag{5}$$

as elaborated in the Supplemental Material [6]. Such transverse-field kicks can be generated by microwave fields, shown as the red circle in Fig. 4 [50].

To realize the next evolution step $U_2^{\rm Floq}$, the Rydberg dressing for $U_1^{\rm Floq}$ is turned off immediately, and another microwave field (brown circle in Fig. 4) is turned on to generate the transverse field $\hat{H}_X(F)=-\sum_j F\hat{\sigma}_j^x$ [50]. At the same time, a strong laser is shone on $|\uparrow\rangle$ such as to excite it to another state $|6P_{3/2},F=5\rangle$, leading to effective laser-induced loss $\hat{H}_Z(g)=\sum_j ig\hat{\sigma}_j^z$ with imaginary field or decay rate $g$ [6,52,54,55,103,104].

After repeatedly alternating between Floquet steps $U_1^{\mathrm{Floq}}$ and $U_2^{\mathrm{Floq}}$ (Fig. 4) over $N = (TJ/J_0\tau_J)$ iterations, the dynamically evolved magnetization $M_x(T)$ can be obtained by measuring the normalized populations in the $|\uparrow\rangle$ and $|\downarrow\rangle$ levels [6,14]. The YLES can be observed as kinks in $M_x(T)$ as $\tau_\gamma$ or $g$ are tuned (Fig. 3). From that, the associated anomalous scaling behavior and exponents [Eq. (2)] can be simply be extracted by controlling the number of trapped atoms $L$ [39,105].

*Discussions.*—The ground state properties of non-Hermitian quantum systems are often deemed experimentally inaccessible due to overwhelming decoherence or the lack of thermal equilibrium. Yet, for the Yang-Lee phase transition in our model, we found that the spontaneously broken $\mathcal{PT}$ symmetry can give rise to pronounced kinks in the dynamical magnetization $M_x(T)$ *without* the need for reaching thermal equilibrium. As such, we provide a realistic Floquet evolution protocol for observing the YLES criticality in a Rydberg chain, distinct from the observation of partition function zeroes in previous experiments [10–12]. Our proposal paves the way for future experimental observation of not just the YLES, but also other nonunitary phase transitions [104,106–110].

The rapid development of universal quantum computation also opens up the possibility of implementing our YLES measurement protocol in quantum computers via ancilla-based methods [111–115]. Moreover, we achieved precise long-time dynamics through our MPS approach for nonunitary circuits. This approach, which is related to mid-circuit measurements [116–119], offers a route to improve the current ancilla-based methods for dynamically simulating various non-Hermitian many-body phenomena [120–127] and unconventional non-Hermitian topology [128–141], on quantum circuits.

All data and code of this work are available from the corresponding authors upon reasonable request.

T. C. thanks Bo Yang for discussions. The exact diagonalization is computed with QuSpin Python library [142,143], and MPS results are calculated with ITensor [144]. T. C. acknowledges support from the National Research Foundation, Singapore under the NRF Fellowship Award (NRF-NRFF12-2020-005). F. Q. is supported by the QEP2.0 grant from the Singapore National Research Foundation (Grant No. NRF2021-QEP2-02-P09) and the MOE Tier-II grant (Proposal ID T2EP50222-0008). This research is supported by the National Research Foundation, Singapore and A*STAR under its CQT Bridging Grant.

*e0554228@u.nus.edu
†tianqi.chen@ntu.edu.sg
‡e0382015@u.nus.edu
§phylohh@nus.edu.sg
‖phylch@nus.edu.sg

[1] C.-N. Yang and T.-D. Lee, Statistical theory of equations of state and phase transitions. I. Theory of condensation, Phys. Rev. **87**, 404 (1952).
[2] T.-D. Lee and C.-N. Yang, Statistical theory of equations of state and phase transitions. II. Lattice gas and Ising model, Phys. Rev. **87**, 410 (1952).
[3] J. L. Cardy, Conformal Invariance and the Yang-Lee Edge Singularity in Two Dimensions, Phys. Rev. Lett. **54**, 1354 (1985).
[4] G. Von Gehlen, Critical and off-critical conformal analysis of the Ising quantum chain in an imaginary field, J. Phys. A **24**, 5371 (1991).
[5] S.-K. Jian, Z.-C. Yang, Z. Bi, and X. Chen, Yang-Lee edge singularity triggered entanglement transition, Phys. Rev. B **104**, L161107 (2021).
[6] See Supplemental Material at http://link.aps.org/supplemental/10.1103/PhysRevLett.131.080403 for details of our experimental proposal and numerical method.
[7] M. E. Fisher, Yang-Lee edge behavior in one-dimensional systems, Prog. Theor. Phys. Suppl. **69**, 14 (1980).
[8] N. Matsumoto, M. Nakagawa, and M. Ueda, Embedding the Yang-Lee quantum criticality in open quantum systems, Phys. Rev. Res. **4**, 033250 (2022).
[9] S. Yin, G.-Y. Huang, C.-Y. Lo, and P. Chen, Kibble-Zurek Scaling in the Yang-Lee Edge Singularity, Phys. Rev. Lett. **118**, 065701 (2017).
[10] X. Peng, H. Zhou, B.-B. Wei, J. Cui, J. Du, and R.-B. Liu, Experimental Observation of Lee-Yang Zeros, Phys. Rev. Lett. **114**, 010601 (2015).
[11] A. Francis, D. Zhu, C. Huerta Alderete, S. Johri, X. Xiao, J. K. Freericks, C. Monroe, N. M. Linke, and A. F. Kemper, Many-body thermodynamics on quantum computers via partition function zeros, Sci. Adv. **7**, eabf2447 (2021).
[12] B.-B. Wei and R.-B. Liu, Lee-Yang Zeros and Critical Times in Decoherence of a Probe Spin Coupled to a Bath, Phys. Rev. Lett. **109**, 185701 (2012).
[13] L. Ding, K. Shi, Q. Zhang, D. Shen, X. Zhang, and W. Zhang, Experimental Determination of $p$ $t$-Symmetric Exceptional Points in a Single Trapped Ion, Phys. Rev. Lett. **126**, 083604 (2021).
[14] L. Zhou, H. Li, W. Yi, and X. Cui, Engineering non-Hermitian skin effect with band topology in ultracold gases, Commun. Phys. **5**, 252 (2022).
[15] Q. Liang, D. Xie, Z. Dong, H. Li, H. Li, B. Gadway, W. Yi, and B. Yan, Dynamic Signatures of Non-Hermitian Skin Effect and Topology in Ultracold Atoms, Phys. Rev. Lett. **129**, 070401 (2022).
[16] N. Malossi, M. M. Valado, S. Scotto, P. Huillery, P. Pillet, D. Ciampini, E. Arimondo, and O. Morsch, Full Counting Statistics and Phase Diagram of a Dissipative Rydberg Gas, Phys. Rev. Lett. **113**, 023006 (2014).
[17] E. A. Goldschmidt, T. Boulier, R. C. Brown, S. B. Koller, J. T. Young, A. V. Gorshkov, S. Rolston, and J. V. Porto, Anomalous Broadening in Driven Dissipative Rydberg Systems, Phys. Rev. Lett. **116**, 113001 (2016).
[18] J. Li, A. K. Harter, J. Liu, L. de Melo, Y. N. Joglekar, and L. Luo, Observation of parity-time symmetry breaking transitions in a dissipative Floquet system of ultracold atoms, Nat. Commun. **10**, 1 (2019).

[19] Z. Ren, D. Liu, E. Zhao, C. He, K. K. Pak, J. Li, and G.-B. Jo, Chiral control of quantum states in non-Hermitian spin–orbit-coupled fermions, Nat. Phys. **18**, 385 (2022).
[20] Q. Liang, D. Xie, Z. Dong, H. Li, H. Li, B. Gadway, W. Yi, and B. Yan, Observation of Non-Hermitian Skin Effect and Topology in Ultracold Atoms, Phys. Rev. Lett. **129**, 070401 (2022).
[21] I. Bloch, Ultracold quantum gases in optical lattices, Nat. Phys. **1**, 23 (2005).
[22] I. Bloch, J. Dalibard, and W. Zwerger, Many-body physics with ultracold gases, Rev. Mod. Phys. **80**, 885 (2008).
[23] S. Giorgini, L. P. Pitaevskii, and S. Stringari, Theory of ultracold atomic Fermi gases, Rev. Mod. Phys. **80**, 1215 (2008).
[24] I. Bloch, J. Dalibard, and S. Nascimbene, Quantum simulations with ultracold quantum gases, Nat. Phys. **8**, 267 (2012).
[25] S. Geier, N. Thaicharoen, C. Hainaut, T. Franz, A. Salzinger, A. Tebben, D. Grimshandl, G. Zürn, and M. Weidemüller, Floquet Hamiltonian engineering of an isolated many-body spin system, Science **374**, 1149 (2021).
[26] P. Scholl, H. J. Williams, G. Bornet, F. Wallner, D. Barredo, L. Henriet, A. Signoles, C. Hainaut, T. Franz, S. Geier *et al.*, Microwave engineering of programmable x x z Hamiltonians in arrays of Rydberg atoms, PRX Quantum **3**, 020303 (2022).
[27] H. Miyake, G. A. Siviloglou, C. J. Kennedy, W. C. Burton, and W. Ketterle, Realizing the Harper Hamiltonian with Laser-Assisted Tunneling in Optical Lattices, Phys. Rev. Lett. **111**, 185302 (2013).
[28] G. Jotzu, M. Messer, R. Desbuquois, M. Lebrat, T. Uehlinger, D. Greif, and T. Esslinger, Experimental realization of the topological Haldane model with ultracold fermions, Nature (London) **515**, 237 (2014).
[29] M. Greiner, O. Mandel, T. Esslinger, T. W. Hänsch, and I. Bloch, Quantum phase transition from a superfluid to a Mott insulator in a gas of ultracold atoms, Nature (London) **415**, 39 (2002).
[30] A. Mazurenko, C. S. Chiu, G. Ji, M. F. Parsons, M. Kanász-Nagy, R. Schmidt, F. Grusdt, E. Demler, D. Greif, and M. Greiner, A cold-atom Fermi-Hubbard antiferromagnet, Nature (London) **545**, 462 (2017).
[31] G. Salomon, J. Koepsell, J. Vijayan, T. A. Hilker, J. Nespolo, L. Pollet, I. Bloch, and C. Gross, Direct observation of incommensurate magnetism in Hubbard chains, Nature (London) **565**, 56 (2019).
[32] M. Schreiber, S. S. Hodgman, P. Bordia, H. P. Lüschen, M. H. Fischer, R. Vosk, E. Altman, U. Schneider, and I. Bloch, Observation of many-body localization of interacting fermions in a quasirandom optical lattice, Science **349**, 842 (2015).
[33] A. Kyprianidis, F. Machado, W. Morong, P. Becker, K. S. Collins, D. V. Else, L. Feng, P. W. Hess, C. Nayak, G. Pagano *et al.*, Observation of a prethermal discrete time crystal, Science **372**, 1192 (2021).
[34] D. Barredo, H. Labuhn, S. Ravets, T. Lahaye, A. Browaeys, and C. S. Adams, Coherent Excitation Transfer in a Spin Chain of Three Rydberg Atoms, Phys. Rev. Lett. **114**, 113002 (2015).
[35] H. Labuhn, D. Barredo, S. Ravets, S. De Léséleuc, T. Macrì, T. Lahaye, and A. Browaeys, Tunable two-dimensional arrays of single Rydberg atoms for realizing quantum Ising models, Nature (London) **534**, 667 (2016).
[36] J. Zeiher, J.-y. Choi, A. Rubio-Abadal, T. Pohl, R. Van Bijnen, I. Bloch, and C. Gross, Coherent Many-Body Spin Dynamics in a Long-Range Interacting Ising Chain, Phys. Rev. X **7**, 041063 (2017).
[37] S. de Léséleuc, D. Barredo, V. Lienhard, A. Browaeys, and T. Lahaye, Optical Control of the Resonant Dipole-Dipole Interaction Between Rydberg Atoms, Phys. Rev. Lett. **119**, 053202 (2017).
[38] C.-J. Lin and O. I. Motrunich, Exact Quantum Many-Body Scar States in the Rydberg-Blockaded Atom Chain, Phys. Rev. Lett. **122**, 173401 (2019).
[39] A. Browaeys and T. Lahaye, Many-body physics with individually controlled Rydberg atoms, Nat. Phys. **16**, 132 (2020).
[40] C.-J. Lin, V. Calvera, and T. H. Hsieh, Quantum many-body scar states in two-dimensional Rydberg atom arrays, Phys. Rev. B **101**, 220304(R) (2020).
[41] V. F. Borish, Many-body spin dynamics with Rydberg-dressed atoms, Ph.D. thesis, Stanford University, 2020.
[42] D. Bluvstein, A. Omran, H. Levine, A. Keesling, G. Semeghini, S. Ebadi, T. T. Wang, A. A. Michailidis, N. Maskara, W. W. Ho *et al.*, Controlling quantum many-body dynamics in driven Rydberg atom arrays, Science **371**, 1355 (2021).
[43] I. Bouchoule and K. Mølmer, Spin squeezing of atoms by the dipole interaction in virtually excited Rydberg states, Phys. Rev. A **65**, 041803(R) (2002).
[44] J. E. Johnson and S. L. Rolston, Interactions between Rydberg-dressed atoms, Phys. Rev. A **82**, 033412 (2010).
[45] N. Henkel, R. Nath, and T. Pohl, Three-Dimensional Roton Excitations and Supersolid Formation in Rydberg-Excited Bose-Einstein Condensates, Phys. Rev. Lett. **104**, 195302 (2010).
[46] G. Pupillo, A. Micheli, M. Boninsegni, I. Lesanovsky, and P. Zoller, Strongly Correlated Gases of Rydberg-Dressed Atoms: Quantum and Classical Dynamics, Phys. Rev. Lett. **104**, 223002 (2010).
[47] H. Schempp, G. Günter, S. Wüster, M. Weidemüller, and S. Whitlock, Correlated Exciton Transport in Rydberg-Dressed-Atom Spin Chains, Phys. Rev. Lett. **115**, 093002 (2015).
[48] J. Zeiher, R. Van Bijnen, P. Schauß, S. Hild, J.-y. Choi, T. Pohl, I. Bloch, and C. Gross, Many-body interferometry of a Rydberg-dressed spin lattice, Nat. Phys. **12**, 1095 (2016).
[49] Y.-Y. Jau, A. Hankin, T. Keating, I. H. Deutsch, and G. Biedermann, Entangling atomic spins with a Rydberg-dressed spin-flip blockade, Nat. Phys. **12**, 71 (2016).
[50] V. Borish, O. Marković, J. A. Hines, S. V. Rajagopal, and M. Schleier-Smith, Transverse-Field Ising Dynamics in a Rydberg-Dressed Atomic Gas, Phys. Rev. Lett. **124**, 063601 (2020).

[51] S. Hollerith, K. Srakaew, D. Wei, A. Rubio-Abadal, D. Adler, P. Weckesser, A. Kruckenhauser, V. Walther, R. van Bijnen, J. Rui *et al.*, Realizing Distance-Selective Interactions in a Rydberg-Dressed Atom Array, Phys. Rev. Lett. **128**, 113602 (2022).

[52] W. Lee, M. Kim, H. Jo, Y. Song, and J. Ahn, Coherent and dissipative dynamics of entangled few-body systems of Rydberg atoms, Phys. Rev. A **99**, 043404 (2019).

[53] L. Li, C. H. Lee, and J. Gong, Topological Switch for Non-Hermitian Skin Effect in Cold-Atom Systems with Loss, Phys. Rev. Lett. **124**, 250402 (2020).

[54] P. Bienias, J. Douglas, A. Paris-Mandoki, P. Titum, I. Mirgorodskiy, C. Tresp, E. Zeuthen, M. J. Gullans, M. Manzoni, S. Hofferberth *et al.*, Photon propagation through dissipative Rydberg media at large input rates, Phys. Rev. Res. **2**, 033049 (2020).

[55] T. M. Wintermantel, Y. Wang, G. Lochead, S. Shevate, G. K. Brennen, and S. Whitlock, Unitary and Nonunitary Quantum Cellular Automata with Rydberg Arrays, Phys. Rev. Lett. **124**, 070503 (2020).

[56] F. Qin, R. Shen, C. H. Lee *et al.*, Non-Hermitian squeezed polarons, Phys. Rev. A **107**, L010202 (2023).

[57] S. Lapp, F. A. An, B. Gadway *et al.*, Engineering tunable local loss in a synthetic lattice of momentum states, New J. Phys. **21**, 045006 (2019).

[58] G. L. Giorgi, Spontaneous *pt* symmetry breaking and quantum phase transitions in dimerized spin chains, Phys. Rev. B **82**, 052404 (2010).

[59] A. Galda and V. M. Vinokur, Parity-time symmetry breaking in spin chains, Phys. Rev. B **97**, 201411(R) (2018).

[60] X. Wang, T. Liu, Y. Xiong, and P. Tong, Spontaneous $\mathcal{PT}$-symmetry breaking in non-Hermitian Kitaev and extended Kitaev models, Phys. Rev. A **92**, 012116 (2015).

[61] T. Tuloup, R. W. Bomantara, C. H. Lee, and J. Gong, Nonlinearity induced topological physics in momentum space and real space, Phys. Rev. B **102**, 115411 (2020).

[62] F. Schäfer, T. Fukuhara, S. Sugawa, Y. Takasu, and Y. Takahashi, Tools for quantum simulation with ultracold atoms in optical lattices, Nat. Rev. Phys. **2**, 411 (2020).

[63] C. Li, G. Zhang, X. Z. Zhang, and Z. Song, Conventional quantum phase transition driven by a complex parameter in a non-Hermitian $\mathcal{PT}$-symmetric Ising model, Phys. Rev. A **90**, 012103 (2014).

[64] D. P. Pires and T. Macrì, Probing phase transitions in non-Hermitian systems with multiple quantum coherences, Phys. Rev. B **104**, 155141 (2021).

[65] S. Sachdev, *Quantum Phase Transitions* (Cambridge University Press, Cambridge, 1999).

[66] S. Sachdev, The quantum Ising model, in *Quantum Phase Transitions*, 2nd ed. (Cambridge University Press, Cambridge, England, 2011), pp. 58–78.

[67] C.-W. Liu, A. Polkovnikov, A. W. Sandvik, and A. P. Young, Universal dynamic scaling in three-dimensional Ising spin glasses, Phys. Rev. E **92**, 022128 (2015).

[68] P. Silvi, G. Morigi, T. Calarco, and S. Montangero, Crossover from Classical to Quantum Kibble-Zurek Scaling, Phys. Rev. Lett. **116**, 225701 (2016).

[69] B.-B. Wei, Probing conformal invariant of non-unitary two-dimensional systems by central spin decoherence, Sci. Rep. **8**, 3080 (2018).

[70] B. Dóra, M. Heyl, and R. Moessner, The Kibble-Zurek mechanism at exceptional points, Nat. Commun. **10**, 1 (2019).

[71] L. Xiao, D. Qu, K. Wang, H.-W. Li, J.-Y. Dai, B. Dóra, M. Heyl, R. Moessner, W. Yi, and P. Xue, Non-Hermitian Kibble-Zurek mechanism with tunable complexity in single-photon interferometry, PRX Quantum **2**, 020313 (2021).

[72] A. Haldar, K. Mallayya, M. Heyl, F. Pollmann, M. Rigol, and A. Das, Signatures of Quantum Phase Transitions After Quenches in Quantum Chaotic One-Dimensional Systems, Phys. Rev. X **11**, 031062 (2021).

[73] In our proposed Rydberg array, we initialize the $|\psi(0)\rangle = |{\leftarrow}{\leftarrow}{\leftarrow}\ldots\ldots\rangle_y$ state for a better implementation of interactions, but the two initial states are both eligible [6].

[74] K. Brandner, V. F. Maisi, J. P. Pekola, J. P. Garrahan, and C. Flindt, Experimental Determination of Dynamical Lee-Yang Zeros, Phys. Rev. Lett. **118**, 180601 (2017).

[75] M. E. Fisher, Yang-Lee Edge Singularity and $\phi$ 3 Field Theory, Phys. Rev. Lett. **40**, 1610 (1978).

[76] K. Uzelac, P. Pfeuty, and R. Jullien, Yang-Lee Edge Singularity from a Real-Space Renormalization-Group Method, Phys. Rev. Lett. **43**, 805 (1979).

[77] G. von Gehlen and A. Honecker, Multi-particle structure in the Zn-chiral Potts models, J. Phys. A **26**, 1275 (1993).

[78] M. Suzuki, Fractal decomposition of exponential operators with applications to many-body theories and Monte Carlo simulations, Phys. Lett. A **146**, 319 (1990).

[79] S. R. White, Density Matrix Formulation for Quantum Renormalization Groups, Phys. Rev. Lett. **69**, 2863 (1992).

[80] G. Vidal, Efficient Simulation of One-Dimensional Quantum Many-Body Systems, Phys. Rev. Lett. **93**, 040502 (2004).

[81] S. R. White and A. E. Feiguin, Real-Time Evolution Using the Density Matrix Renormalization Group, Phys. Rev. Lett. **93**, 076401 (2004).

[82] In this work, we only consider open boundary conditions, which is less costly for MPS calculations.

[83] C. P. Williams, Probabilistic nonunitary quantum computing, *Quantum Information and Computation II* (SPIE, 2004), pp. 297–306.

[84] B. Koczor and S. C. Benjamin, Quantum natural gradient generalized to nonunitary circuits, Phys. Rev. A **106**, 062416 (2022).

[85] H.-N. Xie, S.-J. Wei, F. Yang, Z.-A. Wang, C.-T. Chen, H. Fan, and G.-L. Long, A probabilistic imaginary time evolution algorithm based on non-unitary quantum circuit, arXiv:2210.05293.

[86] A. Daskin and S. Kais, An ancilla-based quantum simulation framework for non-unitary matrices, Quantum Inf. Process. **16**, 1 (2017).

[87] In this limit of Trotterization, the first order correction can sometimes already give rise to interesting new phenomena [88–93], particularly in many-body settings [94–96]. Details of Floquet cycles are shown in [6] and Refs. [49,97–101].

[88] T. Čadež, R. Mondaini, and P. D. Sacramento, Dynamical localization and the effects of aperiodicity in floquet systems, Phys. Rev. B **96**, 144301 (2017).

[89] L. Li, C. H. Lee, and J. Gong, Realistic Floquet Semimetal with Exotic Topological Linkages Between Arbitrarily Many Nodal Loops, Phys. Rev. Lett. **121**, 036401 (2018).

[90] M. S. Rudner and N. H. Lindner, Floquet topological insulators: From band structure engineering to novel non-equilibrium quantum phenomena, arXiv:1909.02008.

[91] F. Nathan, R. Ge, S. Gazit, M. Rudner, and M. Kolodrubetz, Quasiperiodic Floquet-Thouless Energy Pump, Phys. Rev. Lett. **127**, 166804 (2021).

[92] A. Castro, U. De Giovannini, S. A. Sato, H. Hübener, and A. Rubio, Floquet engineering the band structure of materials with optimal control theory, Phys. Rev. Res. **4**, 033213 (2022).

[93] F. Qin, C. H. Lee, R. Chen *et al.*, Light-induced phase crossovers in a quantum spin Hall system, Phys. Rev. B **106**, 235405 (2022).

[94] T. Kuwahara, T. Mori, and K. Saito, Floquet–magnus theory and generic transient dynamics in periodically driven many-body quantum systems, Ann. Phys. (Amsterdam) **367**, 96 (2016).

[95] C. H. Lee, W. W. Ho, B. Yang, J. Gong, and Z. Papić, Floquet Mechanism for Non-Abelian Fractional Quantum Hall States, Phys. Rev. Lett. **121**, 237401 (2018).

[96] B. Ye, F. Machado, and N. Y. Yao, Floquet Phases of Matter via Classical Prethermalization, Phys. Rev. Lett. **127**, 140603 (2021).

[97] D. A. Steck, Quantum and atom optics (2007).

[98] T. Macrì, A. Smerzi, and L. Pezzè, Loschmidt echo for quantum metrology, Phys. Rev. A **94**, 010102(R) (2016).

[99] K. McDonnell, L. F. Keary, and J. D. Pritchard, Demonstration of a Quantum Gate Using Electromagnetically Induced Transparency, Phys. Rev. Lett. **129**, 200501 (2022).

[100] T. Graham, Y. Song, J. Scott, C. Poole, L. Phuttitarn, K. Jooya, P. Eichler, X. Jiang, A. Marra, B. Grinkemeyer *et al.*, Multi-qubit entanglement and algorithms on a neutral-atom quantum computer, Nature (London) **604**, 457 (2022).

[101] J. A. Hines, S. V. Rajagopal, G. L. Moreau, M. D. Wahrman, N. A. Lewis, O. Marković, and M. Schleier-Smith, Spin squeezing by Rydberg dressing in an array of atomic ensembles, arXiv:2303.08805.

[102] J. B. Balewski, A. T. Krupp, A. Gaj, S. Hofferberth, R. Löw, and T. Pfau, Rydberg dressing: Understanding of collective many-body effects and implications for experiments, New J. Phys. **16**, 063012 (2014).

[103] M. Saffman, T. G. Walker, and K. Mølmer, Quantum information with Rydberg atoms, Rev. Mod. Phys. **82**, 2313 (2010).

[104] J. A. S. Lourenço, G. Higgins, C. Zhang, M. Hennrich, and T. Macrì, Non-Hermitian dynamics and $\mathcal{PT}$-symmetry breaking in interacting mesoscopic Rydberg platforms, Phys. Rev. A **106**, 023309 (2022).

[105] P. Scholl, M. Schuler, H. J. Williams, A. A. Eberharter, D. Barredo, K.-N. Schymik, V. Lienhard, L.-P. Henry, T. C. Lang, T. Lahaye *et al.*, Quantum simulation of 2d antiferromagnets with hundreds of Rydberg atoms, Nature (London) **595**, 233 (2021).

[106] L. Zhou, Q.-h. Wang, H. Wang, and J. Gong, Dynamical quantum phase transitions in non-Hermitian lattices, Phys. Rev. A **98**, 022129 (2018).

[107] K. Wang, X. Qiu, L. Xiao, X. Zhan, Z. Bian, B. C. Sanders, W. Yi, and P. Xue, Observation of emergent momentum-time skyrmions in parity–time-symmetric non-unitary quench dynamics, Nat. Commun. **10**, 1 (2019).

[108] R. Hamazaki, Exceptional dynamical quantum phase transitions in periodically driven systems, Nat. Commun. **12**, 1 (2021).

[109] P. Zhang, C. Liu, S.-K. Jian, and X. Chen, Universal entanglement transitions of free fermions with long-range non-unitary dynamics, Quantum **6**, 723 (2022).

[110] Q. Lin, T. Li, L. Xiao, K. Wang, W. Yi, and P. Xue, Topological Phase Transitions and Mobility Edges in Non-Hermitian Quasicrystals, Phys. Rev. Lett. **129**, 113601 (2022).

[111] S.-H. Lin, R. Dilip, A. G. Green, A. Smith, and F. Pollmann, Real-and imaginary-time evolution with compressed quantum circuits, PRX Quantum **2**, 010342 (2021).

[112] J. M. Koh, T. Tai, Y. H. Phee, W. E. Ng, and C. H. Lee, Stabilizing multiple topological fermions on a quantum computer, npj Quantum Inf. **8**, 1 (2022).

[113] J. M. Koh, T. Tai, and C. H. Lee, Simulation of Interaction-Induced Chiral Topological Dynamics on a Digital Quantum Computer, Phys. Rev. Lett. **129**, 140502 (2022).

[114] T. Chen, R. Shen, C. H. Lee, and B. Yang, High-fidelity realization of the AKLT state on a NISQ-era quantum processor, arXiv:2210.13840.

[115] J. M. Koh, T. Tai, and C. H. Lee, Observation of higher-order topological states on a quantum computer, arXiv:2303.02179.

[116] J. M. Pino, J. M. Dreiling, C. Figgatt, J. P. Gaebler, S. A. Moses, M. Allman, C. Baldwin, M. Foss-Feig, D. Hayes, K. Mayer *et al.*, Demonstration of the trapped-ion quantum ccd computer architecture, Nature (London) **592**, 209 (2021).

[117] L. Egan, D. M. Debroy, C. Noel, A. Risinger, D. Zhu, D. Biswas, M. Newman, M. Li, K. R. Brown, M. Cetina *et al.*, Fault-tolerant control of an error-corrected qubit, Nature (London) **598**, 281 (2021).

[118] K. Bharti, A. Cervera-Lierta, T. H. Kyaw, T. Haug, S. Alperin-Lea, A. Anand, M. Degroote, H. Heimonen, J. S. Kottmann, T. Menke *et al.*, Noisy intermediate-scale quantum algorithms, Rev. Mod. Phys. **94**, 015004 (2022).

[119] F. Hua, Y. Jin, Y. Chen, J. Lapeyre, A. Javadi-Abhari, and E. Z. Zhang, Exploiting qubit reuse through mid-circuit measurement and reset, arXiv:2211.01925.

[120] A. Le Boité, G. Orso, and C. Ciuti, Steady-State Phases and Tunneling-Induced Instabilities in the Driven Dissipative Bose-Hubbard Model, Phys. Rev. Lett. **110**, 233601 (2013).

[121] L. M. Sieberer, S. D. Huber, E. Altman, and S. Diehl, Dynamical Critical Phenomena in Driven-Dissipative Systems, Phys. Rev. Lett. **110**, 195301 (2013).

[122] C. Joshi, F. Nissen, and J. Keeling, Quantum correlations in the one-dimensional driven dissipative x y model, Phys. Rev. A **88**, 063835 (2013).

[123] H. Landa, M. Schiró, and G. Misguich, Multistability of Driven-Dissipative Quantum Spins, Phys. Rev. Lett. **124**, 043601 (2020).
[124] C.-M. Jian, B. Bauer, A. Keselman, and A. W. Ludwig, Criticality and entanglement in nonunitary quantum circuits and tensor networks of noninteracting fermions, Phys. Rev. B **106**, 134206 (2022).
[125] T. Pistorius, J. Kazemi, and H. Weimer, Quantum Many-Body Dynamics of Driven-Dissipative Rydberg Polaritons, Phys. Rev. Lett. **125**, 263604 (2020).
[126] P. Deuar, A. Ferrier, M. Matuszewski, G. Orso, and M. H. Szymańska, Fully quantum scalable description of driven-dissipative lattice models, PRX Quantum **2**, 010319 (2021).
[127] J. Naji, M. Jafari, R. Jafari, and A. Akbari, Dissipative floquet dynamical quantum phase transition, Phys. Rev. A **105**, 022220 (2022).
[128] N. Okuma, K. Kawabata, K. Shiozaki, and M. Sato, Topological Origin of Non-Hermitian Skin Effects, Phys. Rev. Lett. **124**, 086801 (2020).
[129] C. H. Lee, Many-body topological and skin states without open boundaries, Phys. Rev. B **104**, 195102 (2021).
[130] L.-J. Zhai, G.-Y. Huang, and S. Yin, Nonequilibrium dynamics of the localization-delocalization transition in non-Hermitian Aubry-André model, Phys. Rev. B **106**, 014204 (2022).
[131] L. Li, S. Mu, C. H. Lee, and J. Gong, Quantized classical response from spectral winding topology, Nat. Commun. **12**, 5294 (2021).
[132] L. Li and C. H. Lee, Non-Hermitian pseudo-gaps, Sci. Bull. **67**, 685 (2022).
[133] R. Shen and C. H. Lee, Non-Hermitian skin clusters from strong interactions, Commun. Phys. **5**, 1 (2022).
[134] Y. Fu and Y. Zhang, Anatomy of open-boundary bulk in multiband non-Hermitian systems, Phys. Rev. B **107**, 115412 (2023).
[135] C. H. Lee, Exceptional Bound States and Negative Entanglement Entropy, Phys. Rev. Lett. **128**, 010402 (2022).
[136] K. Kawabata, K. Shiozaki, and S. Ryu, Many-body topology of non-Hermitian systems, Phys. Rev. B **105**, 165137 (2022).
[137] F. Alsallom, L. Herviou, O. V. Yazyev, and M. Brzezińska, Fate of the non-Hermitian skin effect in many-body fermionic systems, Phys. Rev. Res. **4**, 033122 (2022).
[138] F. Qin, Y. Ma, R. Shen, and C. H. Lee, Universal competitive spectral scaling from the critical non-Hermitian skin effect, Phys. Rev. B **107**, 155430 (2023).
[139] T. Yoshida and Y. Hatsugai, Fate of exceptional points under interactions: Reduction of topological classifications, Phys. Rev. B **107**, 075118 (2023).
[140] A. N. Poddubny, Interaction-induced analog of a non-Hermitian skin effect in a lattice two-body problem, Phys. Rev. B **107**, 045131 (2023).
[141] T. Guo, K. Kawabata, R. Nakai, and S. Ryu, Non-Hermitian boost deformation, Phys. Rev. B **108**, 075108 (2023).
[142] P. Weinberg and M. Bukov, QuSpin: A Python package for dynamics and exact diagonalisation of quantum many body systems part I: Spin chains, SciPost Phys. **2**, 003 (2017).
[143] P. Weinberg and M. Bukov, QuSpin: A Python package for dynamics and exact diagonalisation of quantum many body systems. Part II: Bosons, fermions and higher spins, SciPost Phys. **7**, 20 (2019).
[144] M. Fishman, S. R. White, and E. M. Stoudenmire, The ITensor software library for tensor network calculations, SciPost Phys. Codebases 4 (2022).